

# UC Irvine

## UC Irvine Previously Published Works

### Title

Modeling meibum secretion: Alternatives for obstructive Meibomian Gland Dysfunction (MGD).

### Permalink

<https://escholarship.org/uc/item/7mr5f100>

### Authors

Luo, Shangbang

Djotyan, Gagik

Joshi, Rohan

et al.

### Publication Date

2024

### DOI

10.1016/j.jtos.2023.11.005

Peer reviewed



Published in final edited form as:

*Ocul Surf.* 2024 January ; 31: 56–62. doi:10.1016/j.jtos.2023.11.005.

## Modeling meibum secretion: Alternatives for obstructive Meibomian Gland Dysfunction (MGD)

Shangbang Luo<sup>a,b</sup>, Gagik P. Djotyan<sup>c</sup>, Rohan Joshi<sup>a,b</sup>, Tibor Juhasz<sup>a,b</sup>, Donald J. Brown<sup>a</sup>, James V. Jester<sup>a,b,\*</sup>

<sup>a</sup>Department of Ophthalmology, University of California, Irvine, CA, USA

<sup>b</sup>Department of Biomedical Engineering, University of California, Irvine, CA, USA

<sup>c</sup>Institute for Particle & Nuclear Physics, Wigner Research Center, Budapest, Hungary

### Abstract

**Purpose:** While changes in meibum quality are correlated with severity of meibomian gland dysfunction (MGD) and dry eye disease, little is known regarding the mechanics of meibum secretion. The purpose of this study was to develop a finite element model of meibum secretion and evaluate the effect of various factors that might impact meibum delivery to the ocular surface.

**Methods:** A finite element analysis in COMSOL 6.0 was used to simulate the flow of meibum within the gland's terminal excretory duct. Historical normal human meibum rheology data taken over the meibum melting range from fluid (35–40 °C) to solid (25–30 °C) were then used to calculate the minimum yield stress and plastic viscosity of meibum. The effects of meibum melting state, eyelid pressure and terminal duct diameter on meibum flow rates were then systematically investigated.

**Results:** The melting state of meibum from liquid to solid was associated with an increase in the minimum yield stress and plastic viscosity that caused an exponential decrease in meibum flow. Modeling also established that there was a linear correlation between meibum flow rate and eyelid pressure needed to express meibum and the 4th power of the terminal duct radius.

**Conclusions:** Our results suggest that changes in the melting state of meibum from fluid to solid, as well as changes in the radius of the terminal excretory duct and the force exerted by the eyelid can lead to dramatic decreases in the flow of meibum. Together these findings suggest alternative mechanisms for meibomian gland obstruction.

### Keywords

Meibomian gland dysfunction; Finite element analysis; Modeling; Viscosity; Flow rate; Terminal duct; Orifice; Meibum; Eyelid blink pressure; Non-Newtonian

---

\* Corresponding author. 843 Health Sciences Road, University of California, Irvine, CA, 92697-4390, USA. jjester@hs.uci.edu (J.V. Jester).

Declaration of competing interest  
None.

Appendix A. Supplementary data  
Supplementary data to this article can be found online at <https://doi.org/10.1016/j.jtos.2023.11.005>.

## 1. Introduction

Meibomian glands are holocrine glands embedded in the upper and lower eyelids that secrete lipid (meibum) onto the tear film to retard aqueous tear evaporation [1,2]. Importantly, clinical studies have linked obstruction of the meibomian glands to meibomian gland dysfunction (MGD) leading to signs and symptoms of dry eye disease; a common disorder characterized by burning of the eye and blurry vision related to tear film abnormalities, increased tear evaporation, and ocular surface inflammation [3]. Based on early studies of MGD in rabbits, mice, primates and humans [4–7], a general mechanism associated with hyperkeratinization of the meibomian gland orifice causing ductal plugging, dilation, and a disuse acinar atrophy has been proposed as the most common cause of MGD [8].

Notably, recent studies suggest that altered meibum composition can produce similar obstructive changes within the meibomian gland. Specifically, knockout mice lacking expression of acyl-CoA wax alcohol acyltransferase 2 (AWAT2), which is responsible for the synthesis of meibum wax esters [9], and fatty acyl-CoA reductase 2 (FAR2), which affects meibum fatty alcohol synthesis and consequently wax ester synthesis [10], both show plugging and obstruction of the meibomian gland. Since meibum contains predominantly a mixture of wax and cholesterol esters that comprise from 80 to 90 % of the meibum lipid, loss of wax esters that have a lower melting point than cholesterol esters appear to lead to thickening and increased meibum viscosity [11,12]. Interestingly, Shrestha et al. have discovered increased cholesterol esters in meibum from patients with MGD compared to normal subjects and that cholesterol ester composition increases with age [13]. Similar age-related changes in meibum lipids have also been identified by Sullivan et al., concurrent with changes in meibum opacity [14]. Since aging is a major predictor of MGD, these findings together indicate that changes in meibum viscosity may play the major role in meibomian gland obstruction that leads to dry eye disease.

How changes in meibum viscosity affect meibum secretion is not clear. Recent studies by Rosenfeld et al., have shown that meibum is a non-Newtonian fluid, whose viscosity is modified by shear stress [15]. Since secretion of meibum is passive and a function of eyelid blink pressure [16], we tested the hypothesis that changes in meibum melting temperature and viscosity might decrease meibum flow sufficiently to obstruct the gland leading to the development of MGD and dry eye. To evaluate this hypothesis, we have developed a finite element model of meibum secretion based on previous reports describing meibum rheology, meibomian gland structure and eyelid pressure.

## 2. Methods

### 2.1. Defining the geometry of the meibomian gland terminal duct

Meibum outflow through the gland's orifice occurs via a passive secretory mechanism driven by mechanical forces exerted by the orbicularis muscles on the central duct of the meibomian gland that pushes meibum through the terminal excretory duct and orifice of the gland [16]. The terminal duct was modeled in COMSOL, as a cylinder characterized by a radius  $R$  and a length  $L$  (Fig. 1). Based on a recent report by Cui et al. [17], who measured

the diameter and length of the excretory duct using optical coherence tomography and histology, the average maximal inner diameter of the terminal duct measured approximately 100  $\mu\text{m}$  with a length between 890 and 1370  $\mu\text{m}$ . We therefore selected a radius of  $R = 50$   $\mu\text{m}$  and a length of  $L = 1000$   $\mu\text{m}$  as the baseline conditions for modeling the impact of eyelid pressure, and meibum quality on the meibum flow rates, as detailed in Sec. 2.5.

## 2.2. Defining the pressures for driving the meibum flow

To model meibum secretion, we presumed that the external force exerted by the orbicularis muscle on the eye ( $P_{\text{eyelid}}$ ) led to a compensatory and equal increase in the internal pressure of the central duct that could then be applied as the inlet pressure ( $P_{\text{in}}$ ) exerted on meibum at the entrance to terminal duct as shown in Fig. 1. Meibum secretion was then presumed to be driven by the pressure drop between the inlet pressure ( $P_{\text{in}}$ ) at the start of the terminal duct and the outside or atmospheric pressure ( $P_{\text{out}}$ ) at the orifice. The eyelid pressure ( $P_{\text{eyelid}}$ ) was assumed to be equal to the pressure exerted by the eyelid on the eye surface or the change in intraocular pressure (IOP) during an eyelid blink. Typical reported values are presented in Table 1.

## 2.3. Deriving viscosity properties from human meibum rheological data

The rheological data of human meibum, specifically shear viscosity versus shear rate reported by Rosenfeld et al. [15], were extracted using the GRABIT software [25] in MATLAB 2021b (Mathworks, Inc., Natick, MA). To calibrate the x- and y-axes within the software interface, a power index, denoted as  $n$ , was entered to establish the logarithmic scale for data points corresponding to  $10^n$  values. The extracted data points were subsequently converted to a linear scale using the equation  $linear\_data = 10^{log\_data}$ . These linearized data points were then fitted to a Bingham-Papanastasiou (BP) model, using the formula:

$$\eta_a = \eta_p + \frac{\tau_y}{\dot{\gamma}}(1 - e^{-m_p \dot{\gamma}}) \quad (1)$$

where  $\tau_y$  represents the minimum yield stress,  $\eta_p$  denotes plastic viscosity,  $m_p$  is a scale factor, and  $\eta_a$  is the apparent viscosity defined as the shear stress  $\tau$  applied to a fluid divided by the shear rate  $\dot{\gamma}$  [26]. Further details regarding these parameters, along with a brief introduction of the BP model, can be found in Appendix 1.

## 2.4. Setting other model parameters

The density of meibum changes little with temperature and is assumed to be 0.9  $\text{g}/\text{cm}^3$  [27]. The governing equations in COMSOL are the Navier-Stokes equations, considering no-slip boundary conditions. The element size chosen for the mesh was set to 'Normal' in the COMSOL software, resulting in a mesh consisting of approximately 250,000 elements. The flow is assumed to be laminar [28], and in this study, it is modeled as a single-phase, incompressible fluid.

## 2.5. Pressure, geometry, and temperature dependent studies

The inlet pressure influences meibum flow, and therefore, a series of eyelid pressures as discussed in Sec. 2.2 and presented in Table 1 were used to study the pressure-dependent meibum flow behaviors. To evaluate the impact of geometric factors on meibum expression, a range of radiuses ( $R = 12.5, 25, 37.5, 50 \mu\text{m}$ ) was investigated while keeping the length fixed at  $L = 1000 \mu\text{m}$ . While we did not model changes in excretory duct length, it should be noted that the meibum flow rate inversely correlates with length of the duct, as supported by the analytical derivation presented in Appendix 2. Lastly, parametric sweep studies were conducted for viscosities at four different normal meibum melting temperatures (Table 2), with the model's geometry assumed to be fixed at  $R = 50 \mu\text{m}$  and  $L = 1000 \mu\text{m}$ .

## 2.6. Quantifying the meibum secretion

The volumetric flow rate,  $Q$ , was used as a measure of the volume of fluid passing through a specific area per unit of time. It was calculated using the equation:

$$Q = S_c \cdot \bar{u} \quad (2)$$

where  $S_c$  represents the cross-sectional area of the meibum flow through the terminal duct and orifice ( $S_c = \pi R^2$ ), and  $u$  denotes the average velocity obtained from COMSOL simulations. Flow rates were computed and compared under different pressure conditions, geometries, and viscosities over the range of meibum melting temperatures.

## 3. Results

### 3.1. Meibum viscosity parameters for a non-Newtonian model

The resulting fitted rheology data were presented in logarithmic scale as depicted in Fig. 2. In general, it was observed that the data at lower temperatures exhibited a superior fit to the BP model compared to the data at higher temperatures. The fitting parameters obtained from the analysis, namely  $\eta_p$ ,  $\tau_y$ , and  $m_p$ , are presented in Table 2. With the increase in temperature from 25 to 40 °C, meibum undergoes melting, resulting in a significant decrease in both the minimum yield stress and plastic viscosity. Specifically, solid meibum at 25 °C exhibits higher minimum yield stress of 95.53 N/m<sup>2</sup>, and a larger plastic viscosity of 74.95 Pa·s, while more fluid meibum at a melting temperature of 40 °C exhibits dramatically lower minimum yield stress of 2.06 N/m<sup>2</sup> and plastic viscosity of 1.01 Pa·s. The material parameter  $m_p$  could not be accurately fitted using the data at temperatures of 35 and 40 °C. However, at 25 °C, the value of  $m_p$  was relatively large, indicating a more rigid behavior compared to that at 30 °C.

### 3.2. Pressure dependency

When the terminal duct radius was held at 50  $\mu\text{m}$ , there was a strong correlation between meibum flow rate and eyelid pressure that increased with increasing temperature as shown in Fig. 3. The degree of linearity correlated with the meibum temperature and quality, with more fluid meibum (C and D) showing a slightly higher linear correlation compared

to more viscous meibum (A and B). This difference was due to the fact that meibum at lower temperature with higher minimal yield stress and plastic viscosity show practically no meibum flow at the eyelid pressures below 2 kPa.

Previous reports of meibum delivery following eyelid blinking as reported by Chew et al. [27] and Nagymihalyi et al. [29] using a meibometer to measure the casual level of lipid on the eyelid margin, suggest that an average blink delivers from 0.17 to 0.53  $\mu\text{g}$  of meibum per gland to the eyelid margin. While these levels seem to vary widely between individuals, the estimated average meibum flow rate might vary from 0.55 to 1.7 nL/s during a normal blink. Based on modeling and assuming a normal eyelid temperature of 35  $^{\circ}\text{C}$ , this level of meibum flow would be achieved by eyelid pressures varying from 1.1 to 2.1 kPa (Fig. 5).

A time-dependent velocity map video illustrating meibum flow in the terminal duct with a radius of 50  $\mu\text{m}$  that would be induced during eyelid blinking was also generated as shown in the supplementary materials (Video S1). For the video, a typical blink duration of  $1/3 \text{ s}$  ( $T$ ) and a blink interval ( $T$ ) of 5 s [30] were applied, with inlet pressure

$$P_{\text{in}} = \begin{cases} P_r, 0 \leq t < T - \Delta T \\ P_b, T - \Delta T \leq t < T \end{cases}, \text{ where eyelid resting pressure } P_r \text{ (0.4 kPa) and eyelid blink pressure } P_b \text{ (2.1 kPa) at a temperature of } 35 \text{ }^{\circ}\text{C}.$$

$P_b$  (2.1 kPa) at a temperature of 35  $^{\circ}\text{C}$ .

### 3.3. Viscosity effects

Viscosity data of meibum obtained at different melting temperatures (refer to Table 2) were used to examine the influence on meibum expression within a BP model. As the meibum transitioned from fluid to solid, there was an exponential decrease in meibum flow, caused by the increasing minimum yield stress and plastic viscosity (Fig. 4). To visualize both effects of viscosity and eyelid pressure, Fig. 5 presents a compilation of cross-sectional distributions of the velocities and flow rates of meibum secretion from a meibomian gland orifice at different viscosities and eyelid pressures.

### 3.4. Geometric effects

As shown in Fig. 6, there was a significant correlation between meibum flow rate and the fourth power of the duct's radius  $R^4$  at both low (A) and high (B) eyelid blink pressures. A similar relationship was observed in Eq. S14 of Appendix 2.

## 4. Discussion

In this paper we have developed a finite element model for measuring the flow of meibum from the terminal duct of the meibomian gland and analyzed the combined effects of eyelid pressure and duct radius on meibum delivery to the eyelid margin. For this analysis we have modeled meibum as a non-Newtonian fluid based on rheological data of human meibum as reported by Rosenfeld et al. [15]. Minimum yield stress and plastic viscosity values were estimated based on data from meibum taken at different temperature values covering the melting range of meibum from 25  $^{\circ}\text{C}$  to 40  $^{\circ}\text{C}$ . Based on finite element modeling, meibum flow rates exponentially decreased with increasing minimum yield stress and plastic viscosity. Modeling also revealed that meibum flow rates at the same minimum yield stress and plastic viscosity was linearly related to eyelid pressure and the fourth power of the duct

radius. Together, these findings suggest novel alternatives to the classical understanding of obstructive MGD and potentially new mechanisms for meibomian gland atrophy involving changes in meibum melting point, eyelid pressure and ductal radius as discussed below.

#### 4.1. Effects of altered meibum melting point

As measured by Butovich et al. [31], meibum obtained from normal subjects has a wide melting range from 10 °C to 40 °C, with three transition points at 12 °C, 21 °C and 32 °C. On the other hand, meibum from dry eye subjects have a slightly higher range with transition points of 22 °C and 33 °C as measured by Butovich et al. and up to 35 °C as measured by McCulley and Shine [32]. These changes in meibum melting point are also consistent with the decreased presence of wax esters that have been identified in patients with dry eye disease [13,14], and the known lower melting point of wax esters [11,12]. Furthermore, meibum from dry eye patients also contains variable amounts of proteins which may also affect the meibum melting temperature [31,33,34].

As noted in our study, shifts in the melting temperature of meibum has exponential effects on both the minimum yield stress and plastic viscosity that increase more than three to four-fold with a temperature shift of only 5 °C (35 °C–30 °C), resulting in a change from 5 to 24 N/m<sup>2</sup> and 3–10 Pa·s, respectively. These effects of temperature on meibum flow rate predict to large extent the findings of Nagymihalyi et al. [29], which identified a marked decrease in the deposition of meibum after 10 blinks following a 7 °C cooling of the surface of the eyelids. While rheology of meibum from MGD patients with altered meibum quality have not been measured, the measured shift in melting temperature of meibum noted for MGD patients would predict similar increase in the minimum yield stress and plastic viscosity and an exponential decrease in meibum flow that could be reduced by as much as 90 % depending on the eyelid pressure.

#### 4.2. Effects of eyelid pressure on meibum flow rates

A range of eyelid pressures on the eye have been reported using a wide range of techniques from measuring the intraocular pressure during blinking [18–20], to more static measurements using scleral or contact lenses with pressure sensors [21–24] as detailed in Table 1. For the most part, static eyelid pressures with eyelids either open or closed produce very low pressures on the eye that are generally below 10 mmHg (1.3 kPa), while eyelid blinking produces higher values. Reports measuring changes in intraocular pressure during eyelid blinking show much higher changes in IOP that can achieve levels from 40 mmHg to 90 mmHg during squeezing of the eyelids [18,20]. As noted earlier however, translating changes in IOP to the pressure exerted on the eye by the eyelid is difficult. Likewise, measurement of eyelid pressure during blinking using contact lens pressure sensors is complicated by the fact that the sensor needs to be inserted between the eyelid and the eye, thus changing the normal application of force. Furthermore, the force applied to the eye by the eyelid is localized to the lid wiper or distal region of eyelid near to eyelid margin, which may not be adequately measured by some sensors [23]. Finally, the relationship between the pressure the eyelid exerts on the eye and the pressure exerted on the meibomian gland duct is not known. All these concerns make it difficult to extrapolate eyelid pressure data to

pressure changes in the duct of the meibomian gland, other than to say that blink pressure is most likely higher than resting pressure with eyes open or closed.

Nevertheless, modeling demonstrates a linear increase in meibum flow rate with higher eyelid pressures. This observation is consistent with clinical findings and aligns with intuitive expectations. Interestingly, eyelid pressure on the eye has been shown to decrease with age, averaging 23.2 mmHg in individuals that are over twenty, decreasing to 13.6 mmHg for individuals over sixty, or a reduction of 2–3 mmHg for every 10 years [35]. This decrease in eyelid pressure would translate into a 40 % decrease in meibum flow rate for individuals over sixty and a 70 % reduction for individuals over 90 years of age. While the volume of meibum delivered to the eyelid margin with each blink likely exceeds the volume necessary to replenish lipid onto the eyelid surface by some 40 fold [27], this age-related decrease in eyelid pressure combined with changes in melting temperature and other structural changes in the duct may help explain the significant relationship between age and MGD. Certainly, more in-depth modeling of this mechanism is needed in the future.

### 4.3. Effects of ductal morphology on meibum flow rates

When other parameters are held constant, we observe a linear relationship between the flow rate and the fourth power of the duct radius. Both the pressure and geometric studies indicated that the flow of meibum followed Poiseuille's law [28], which is typically derived for a Newtonian fluid. However, we speculate that the non-Newtonian behaviors did not overwhelmingly dominate the entire flow pattern (please refer to Appendix 2 for further information). Interestingly, at temperatures of 35 °C, comparable meibum flow rates were found between (A) a radius of 50  $\mu\text{m}$  and an eyelid pressure of 1.1 kPa, and (B) a radius of 25  $\mu\text{m}$  and an eyelid pressure of 12.3 kPa (Fig. 6).

While hyperkeratinization and plugging of the meibomian gland duct is cited as the most common cause of obstructive MGD, a recent detailed immunohistochemical study of the human meibomian gland by Reneker et al., found evidence of ductal epithelial hyperproliferation but not hyperkeratinization [36]. It is interesting to note that our modeling data also predicts significant effects of ductal epithelial thickening on meibum flow rates. While little is known regarding the thickness of the ductal epithelium that lines the excretory duct, histology images presented by Cui et al. report an outer ductal diameter of 172  $\mu\text{m}$  with an inner diameter of 100  $\mu\text{m}$ , giving a ductal epithelial thickness of approximately 35  $\mu\text{m}$  [17]. Since the excretory duct is embedded in a dense collagenous tarsal plate, it might be assumed that the outer diameter of the excretory duct is fixed, and any hyperproliferation leading to ductal epithelial thickening would lead to a reduction in the inner diameter of the duct. Based on our modeling, an increase in epithelial thickness from 35 to 40  $\mu\text{m}$ , or a 5  $\mu\text{m}$  increase, would lead to a 35 % decrease in meibum flow rate in a 100  $\mu\text{m}$  diameter duct, and a 62 %–86 % decrease in flow rate in a 50  $\mu\text{m}$  diameter duct depending on the eyelid force.

## 5. Limitations

A major limitation of this study is the lack of available data for meibum rheology from both normal and MGD subjects. For normal meibum, rheology data is only available for only 4 discrete melting temperatures from 25 °C to 40 °C [15], while no data is available from

meibum expressed from MGD patients. While we have assumed that changes in meibum melting temperature from MGD patients would translate into changes in meibum flow rates indicative of the increased minimum yield stress and plastic viscosity observed at lower temperature in normal meibum, this may not accurately predict the changes that occur. Additionally, it is crucial to gather more clinical rheology data encompassing the clinical range of altered meibum quality from viscous to toothpaste-like in future studies.

A second limitation of this study is that little is known regarding the actual mechanisms of meibum secretion, and the effect of forces that are exerted on the inside of the duct to push meibum out of the gland. While there are many reports concerning the force the eyelid exerts on the eye, whether these forces are directly related to the compressive forces exerted on the gland are not known. Furthermore, how these forces translate into the pressure exerted on the excretory portion of the duct is not known and whether these forces can produce other effects on the gland remains to be studied. In this report we have only modeled the terminal, 1 mm distal end of the duct, and how this pressure affects the more central duct remains unclear. It is likely that as meibum flow is decreased, internal ductal pressure may have effects on the lateral wall of the common duct causing increased mechanical strain. While ‘acinar disuse atrophy’ is an often-cited mechanism for obstructive MGD [8], a more plausible alternative is that reduced meibum flow regardless of cause leads to increased mechanical strain and stretching of the ductal and acinar cells that cause downstream effects on cell differentiation. To more clearly understand these potential effects, a more complex modeling of the entire meibomian gland is needed, which requires better understanding of the tissue compliance of the ductal epithelium and surrounding extracellular matrix.

## 6. Conclusions

In summary, this study has successfully developed and applied a finite element analysis to simulate the flow of non-Newtonian meibum within the terminal duct of the meibomian gland. Through systematic investigations, the impact of eyelid pressure, meibum minimum yield stress and plastic viscosity, and distal duct geometry on meibum flow rate has been thoroughly explored. The results reveal a significant exponential decrease in meibum flow with increasing minimum yield stress and plastic viscosity that develop over the range of normal meibum melting temperatures from 25 °C to 40 °C. This finding predicts that clinical changes in meibum quality noted in MGD patients can be explained by an increase in the meibum melting temperature causing the appearance of increased meibum viscosity, reduced meibum flow and the requirement for increased application of force to express altered meibum. Our analysis also found that there was a linear relationship between the fourth power of the distal duct radius and the meibum flow rate, indicating that small changes in the thickness of the ductal epithelium may produce significant changes in the flow rate of meibum. Finally, there was a linear relationship between eyelid pressure and meibum flow. Together, changes in these three factors can lead to marked restriction of meibum flow onto the eyelid margin, and, in part, provide an alternative cause for obstructive MGD.

## Supplementary Material

Refer to Web version on PubMed Central for supplementary material.

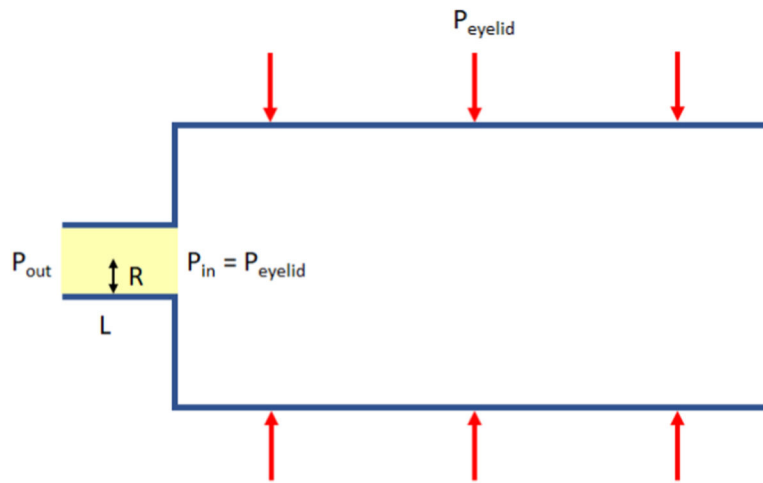
## Funding

Supported in part by grants from the NIH/NEI R01EY021510 (JVJ), NIH/NEI P30EY034070 (JVJ), NIH/NEI R01EY030304 (TJ), Discovery Eye Foundation, an Unrestricted Grant from Research to Prevent Blindness, Inc. (RPB-203478), and the Skirball Program in Molecular Ophthalmology and Basic Science.

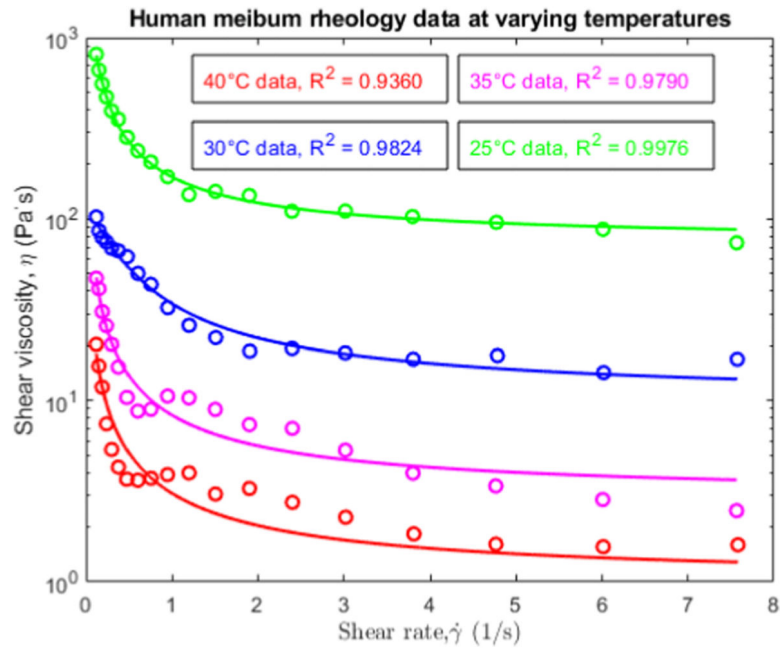
## References

- [1]. Mathers WD, Lane JA. Meibomian gland lipids, evaporation, and tear film stability. *Adv Exp Med Biol* 1998;438:349–60. [PubMed: 9634908]
- [2]. Mishima S, Maurice DM. The oily layer of the tear film and evaporation from the corneal surface. *Exp Eye Res* 1961;1:39–45. [PubMed: 14474548]
- [3]. Tomlinson A, Bron AJ, Korb DR, Amano S, Paugh JR, Pearce EI, et al. The international workshop on meibomian gland dysfunction: report of the diagnosis subcommittee. *Invest Ophthalmol Vis Sci* 2011;52:2006–49. [PubMed: 21450918]
- [4]. Jester JV, Rajagopalan S, Rodrigues M. Meibomian gland changes in the rhino (hrrhrrh) mouse. *Invest Ophthalmol Vis Sci* 1988;29:1190–4. [PubMed: 2458328]
- [5]. Jester JV, Rife L, Nii D, Luttrull JK, Wilson L, Smith RE. In vivo biomicroscopy and photography of meibomian glands in a rabbit model of meibomian gland dysfunction. *Invest Ophthalmol Vis Sci* 1982;22:660–7. [PubMed: 7076409]
- [6]. Anatomy Obata H. and histopathology of human meibomian gland. *Cornea* 2002; 21:S70–4. [PubMed: 12484702]
- [7]. Ohnishi Y, Kohno T. Polychlorinated biphenyls poisoning in monkey eye. *Invest Ophthalmol Vis Sci* 1979;18:981–4. [PubMed: 113362]
- [8]. Foulks GN, Bron AJ. Meibomian gland dysfunction: a clinical scheme for description, diagnosis, classification, and grading. *Ocul Surf* 2003;1:107–26. [PubMed: 17075643]
- [9]. Widjaja-Adhi MAK, Silvaroli JA, Chelstowska S, Trischman T, Bederman I, Sayegh R, et al. Deficiency in Acyl-CoA:Wax Alcohol Acyltransferase 2 causes evaporative dry eye disease by abolishing biosynthesis of wax esters. *Faseb J* 2020; 34:13792–808. [PubMed: 32851726]
- [10]. Otsuka K, Sawai-Ogawa M, Kihara A. Formation of fatty alcohols-components of meibum lipids-by the fatty acyl-CoA reductase FAR2 is essential for dry eye prevention. *Faseb J* 2022;36:e22216.
- [11]. Iyengar BT, Schlenk H. Melting points of synthetic wax esters. *Lipids* 1969;4: 28–30. [PubMed: 5766845]
- [12]. Mahadevan V, Lundberg W. Preparation of cholesterol esters of long-chain fatty acids and characterization of cholesteryl arachidonate. *JLR (J Lipid Res)* 1962;3: 106–10.
- [13]. Shrestha RK, Borchman D, Foulks GN, Yappert MC, Milliner SE. Analysis of the composition of lipid in human meibum from normal infants, children, adolescents, adults, and adults with meibomian gland dysfunction using (1)H-NMR spectroscopy. *Invest Ophthalmol Vis Sci* 2011;52:7350–8. [PubMed: 21849420]
- [14]. Sullivan BD, Evans JE, Dana MR, Sullivan DA. Influence of aging on the polar and neutral lipid profiles in human meibomian gland secretions. *Arch Ophthalmol* 2006;124:1286–92. [PubMed: 16966624]
- [15]. Rosenfeld L, Cerretani C, Leiske DL, Toney MF, Radke CJ, Fuller GG. Structural and rheological properties of meibomian lipid. *Invest Ophthalmol Vis Sci* 2013;54: 2720–32. [PubMed: 23513065]
- [16]. Linton RG, Curnow DH, Riley WJ. The meibomian glands: an investigation into the secretion and some aspects of the physiology. *Br J Ophthalmol* 1961;45:718–23. [PubMed: 18170726]
- [17]. Cui X, Wu Q, Zhai Z, Yang Y, Wei A, Xu J, et al. Comparison of the meibomian gland openings by optical coherence tomography in obstructive meibomian gland dysfunction and normal patients. *J Clin Med* 2020;9. [PubMed: 33374507]
- [18]. Coleman DJ, Trokel S. Direct-recorded intraocular pressure variations in a human subject. *Arch Ophthalmol* 1969;82:637–40. [PubMed: 5357713]

- [19]. Korb DR, Blackie CA. Meibomian gland diagnostic expressibility: correlation with dry eye symptoms and gland location. *Cornea* 2008;27:1142–7. [PubMed: 19034129]
- [20]. van den Bosch J, Pennisi V, Mansouri K, Weinreb RN, Thieme H, Hoffmann MB, et al. Effect of eyelid muscle action and rubbing on telemetrically obtained intraocular pressure in patients with glaucoma with an IOP sensor implant. *Br J Ophthalmol* 2022;107:1425–31. [PubMed: 35701079]
- [21]. Miller D. Pressure of the lid on the eye. *Arch Ophthalmol* 1967;78:328–30. [PubMed: 6040008]
- [22]. Sakai E, Shiraishi A, Yamaguchi M, Ohta K, Ohashi Y. Blepharo-tensiometer: new eyelid pressure measurement system using tactile pressure sensor. *Eye Contact Lens* 2012;38:326–30. [PubMed: 22890227]
- [23]. Shaw AJ, Collins MJ, Davis BA, Carney LG. Eyelid pressure and contact with the ocular surface. *Invest Ophthalmol Vis Sci* 2010;51:1911–7. [PubMed: 19834035]
- [24]. Wang J, Bao J, Song W, Li S, Hao Y, Tian L, et al. Assessment of eyelid pressure using a novel pressure measurement device in patients with moderate-to-severe dry eye disease. *Front Med* 2022;9:833576.
- [25]. Doke J. GRABIT. MATLAB central file exchange. 2023.
- [26]. Papanastasiou TC. Flows of materials with yield. *J Rheol* 1987;31:385–404.
- [27]. Chew CK, Jansweijer C, Tiffany JM, Dikstein S, Bron AJ. An instrument for quantifying meibomian lipid on the lid margin: the Meibometer. *Curr Eye Res* 1993;12:247–54. [PubMed: 8482113]
- [28]. Mitchell JW. Fox and McDonald's Introduction to fluid mechanics. tenth ed. Hoboken, NJ: Wiley; 2020.
- [29]. Nagymihalyi A, Dikstein S, Tiffany JM. The influence of eyelid temperature on the delivery of meibomian oil. *Exp Eye Res* 2004;78:367–70. [PubMed: 15106914]
- [30]. Fatt I, Weissman BA. Physiology of the eye: an introduction to the vegetative functions. second ed. Boston: Butterworth-Heinemann; 1992.
- [31]. Butovich IA, Lu H, McMahon A, Ketelson H, Senchyna M, Meadows D, et al. Biophysical and morphological evaluation of human normal and dry eye meibum using hot stage polarized light microscopy. *Invest Ophthalmol Vis Sci* 2014;55: 87–101. [PubMed: 24282231]
- [32]. McCulley JP, Shine WE. Meibomian secretions in chronic blepharitis. *Adv Exp Med Biol* 1998;438:319–26. [PubMed: 9634903]
- [33]. Ong BL, Hodson SA, Wigham T, Miller F, Larke JR. Evidence for keratin proteins in normal and abnormal human meibomian fluids. *Curr Eye Res* 1991;10:1113–9. [PubMed: 1724955]
- [34]. Palaniappan CK, Schutt BS, Brauer L, Schicht M, Millar TJ. Effects of keratin and lung surfactant proteins on the surface activity of meibomian lipids. *Invest Ophthalmol Vis Sci* 2013;54:2571–81. [PubMed: 23482461]
- [35]. Yamaguchi M, Shiraishi A. Relationship between eyelid pressure and ocular surface disorders in patients with healthy and dry eyes. *Invest Ophthalmol Vis Sci* 2018;59.
- [36]. Reneker LW, Irlmeier RT, Shui YB, Liu Y, Huang AJW. Histopathology and selective biomarker expression in human meibomian glands. *Br J Ophthalmol* 2020;104:999–1004. [PubMed: 31585964]

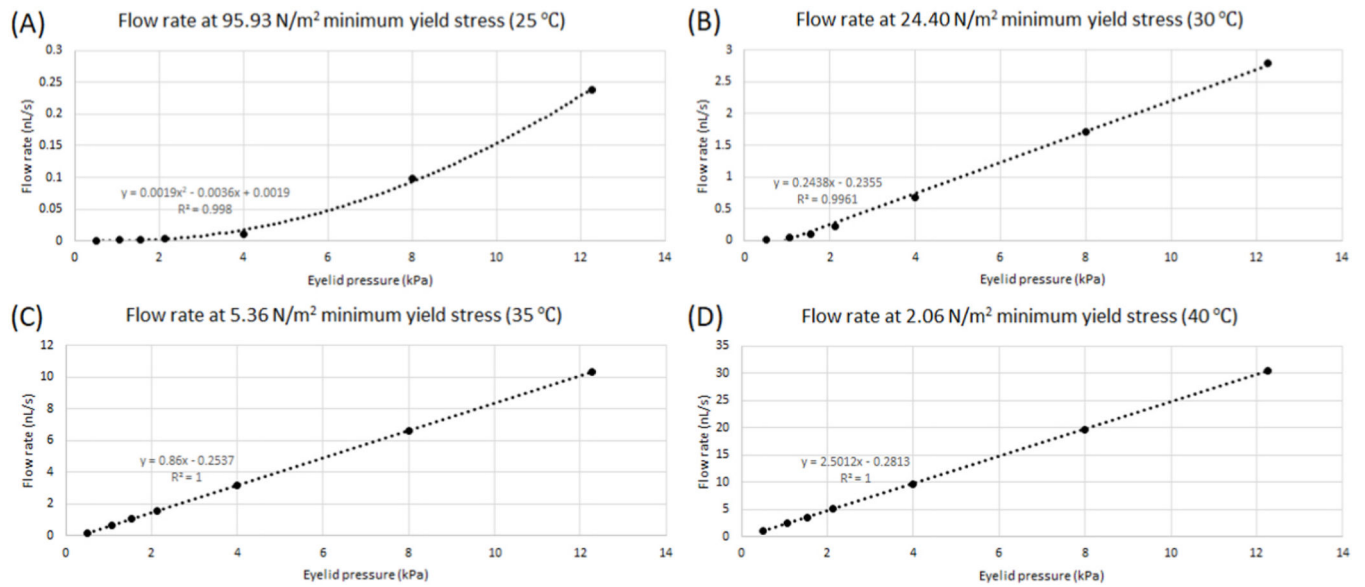


**Fig. 1.** Meibomian gland's terminal duct modeling in COMSOL. Meibum secretion is modeled by assuming that the orbicularis muscle overlying the meibomian glands, but not the terminal excretory duct and orifice, exerts an eyelid pressure ( $P_{\text{eyelid}}$ ) on the meibomian gland duct that is translate to the inlet pressure ( $P_{\text{in}}$ ) of the terminal excretory duct represented as a simplified cylindrical model of a radius ( $R$ ) and a length ( $L$ ). The pressure at the gland orifice is assumed to be the atmospheric pressure ( $P_{\text{out}}$ ). The pressure difference between the two drives the meibum through the terminal duct (depicted as the yellow region). Dimension not scaled.



**Fig. 2.**

The viscosity of human meibum was extracted from existing literature and fitted as a function of shear rate at different temperatures. The coefficient of determination  $R^2$  (not duct radius) was used to evaluate the goodness of the fitting, with a value of 1 indicating an ideal fit between the model and the respective data.

**Fig. 3.**

Impact of eyelid pressure on meibum flow rate from a meibomian gland orifice at different minimum yield stress or plastic viscosity of meibum obtained at different temperatures along the meibum melting curve, (A) 25 °C, (B) 30 °C, (C) 35 °C, and (D) 40 °C. A strong linear correlation exists between the meibum flow rate and the eyelid pressure except in case A. It should be noted that there is no meibum flow at low eyelid pressures (<2 kPa) for high minimum yield stress and plastic viscosity (A and B). Modeling geometry is fixed: R = 50  $\mu$ m, L = 1000  $\mu$ m.

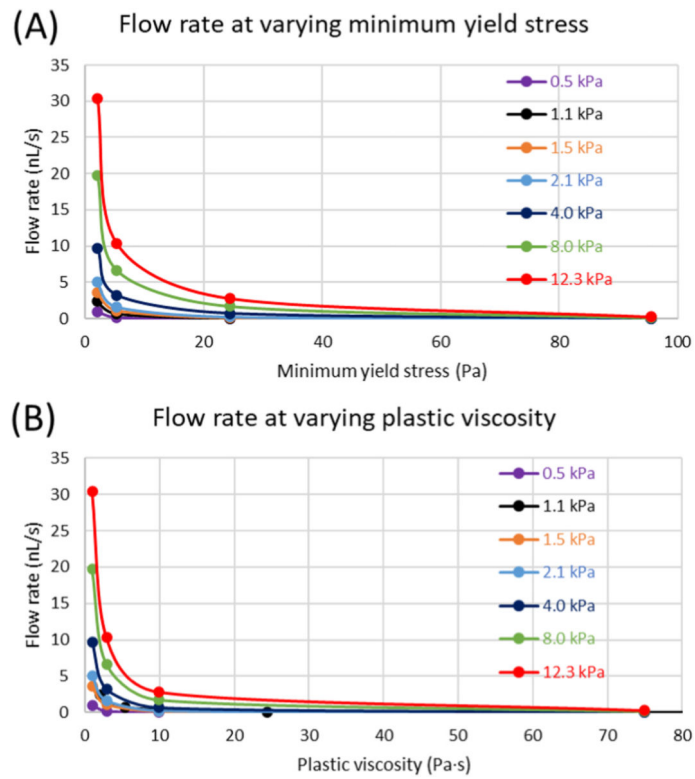


**Fig. 4.** Effects of changes in meibum viscosities on meibum flow rate from a meibomian gland orifice. Note that there is an exponential decrease in meibum flow rates with (A) higher minimum yield stress and (B) plastic viscosity. Different curves indicate modeling under different eyelid pressures.  $R = 50 \mu\text{m}$ ,  $L = 1000 \mu\text{m}$ .

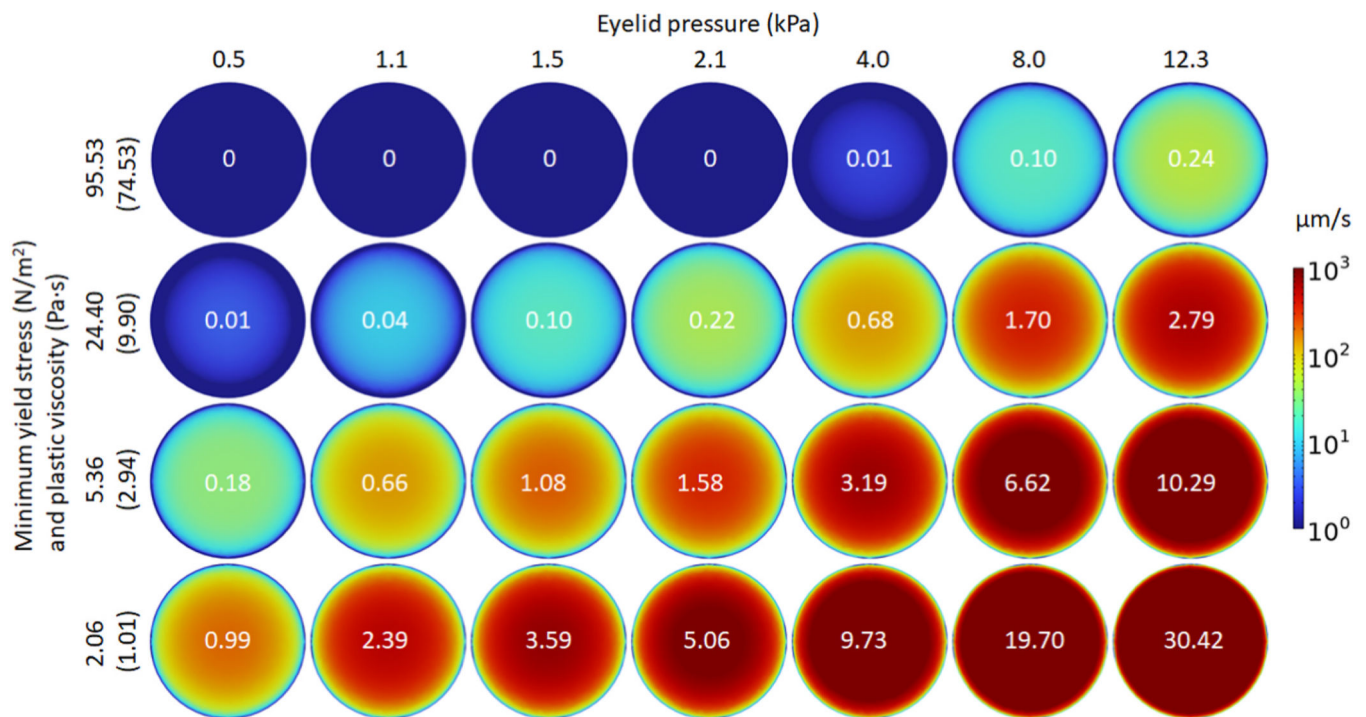


**Fig. 5.**

Cross-sectional distribution of the velocity maps ( $\mu\text{m/s}$ ) and flow rates ( $\text{nL/s}$ ) of meibum secretion from a meibomian gland orifice at different meibum viscosities and eyelid pressures, as summarized in the current study. The velocity is color mapped in a log scale between 1 and 1000  $\mu\text{m/s}$ . No-slip boundary conditions result in zero velocities at the edges of the ducts. Corresponding flow rates are shown in the center of each map. The 7 typical eyelid pressures under current study are selected or approximated from Table 1, and their mmHg values are converted into kPa values.  $R = 50 \mu\text{m}$  and  $L = 1000 \mu\text{m}$ .

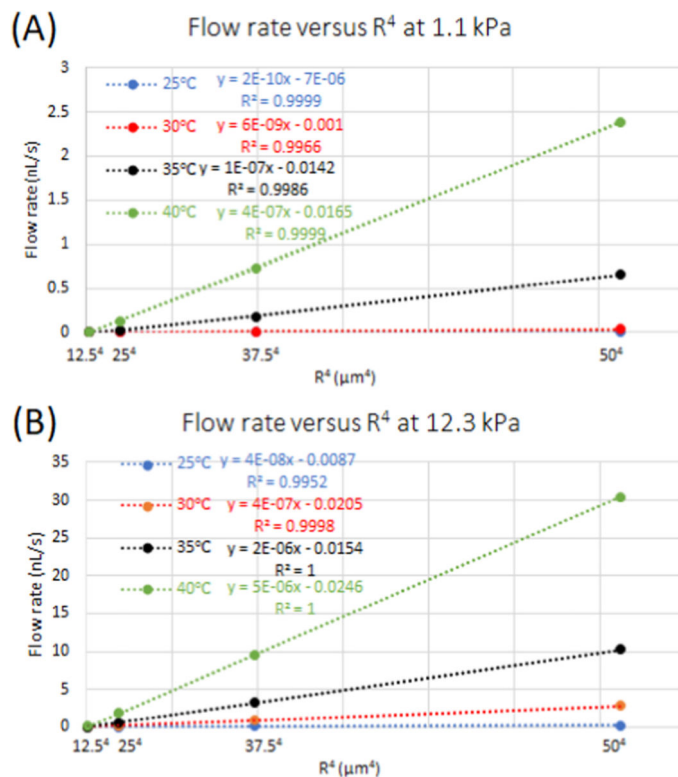


**Fig. 6.** Influence of terminal duct size on meibum flow rate from a meibomian gland orifice. The fittings suggest that the meibum flow rate exhibits a linear correlation with the fourth power of the duct radius, both at low eyelid pressure (A), where  $P_b = 1.1$  kPa, and at high eyelid pressure (B), where  $P_b = 12.3$  kPa. This is consistent with Poiseuille’s Law. At a temperature of 35 °C in scenario (A), with a radius of 50  $\mu\text{m}$  and an eyelid pressure of 1.1 kPa, a comparable meibum flow rate of 0.6 nL/s is observed when compared to scenario (B), which involves a radius of 25  $\mu\text{m}$  and an eyelid pressure of 12.3 kPa. Note that different colors indicate different temperatures.  $L = 1000$   $\mu\text{m}$ .

Table 1

Representative values of eyelid pressures utilized in this study.

Pressure measured	References	pressure change in mmHg	corresponding kPa	eyelid maneuvers	Method
Changes in IOP	Coleman etc, 1969 [18]	90	12	eyelid squeezing	strain gauge
		10	1.3	turning eyes to side	
		10	1.3	blinking	
	Korb etc, 2008 [19]	35	4.7	eyelid squeezing	custom diagnostic instrument
	van den Bosch etc, 2022 [20]	59.1 ± 9.6 42.2 ± 5.8 3.8 ± 0.6 11.6 ± 2.4 0	7.9 ± 1.3 5.6 ± 0.8 0.5 ± 0.1 1.5 ± 0.3 0	eyelid rubbing eyelid squeezing eyelid closure voluntary blink involuntary blink	implanted telemetric IOP sensors in open-angle glaucoma patients
Corneal surface measure	Miller etc, 1967 [21]	10.3 ± 2.3	1.4 ± 0.3	deliberate blink	scleral lens balloon sensor
		7.6 ± 3.5	1.0 ± 0.5	sound blink	
		7.5 ± 2.3	1.0 ± 0.3	touch blink	
		2.8 ± 2.2	0.4 ± 0.3	light blink	
		3.2 ± 1.2	0.4 ± 0.2	static eyelid closure	
		16.95 ± 6.08	2.3 ± 0.8	static eye closed, upper lid	
		16.11 ± 7.27	2.1 ± 1.0	static eye closed, lower lid	
Shaw etc, 2010 [23]	8.0 ± 3.4	1.1 ± 0.5	static eyelid pressure	piezoresistive pressure sensors at upper lids in young adult subjects	
Wang etc, 2022 [24]	3.9 ± 1.2	0.5 ± 0.2	eyelid closed	custom built membrane pressure sensor	

**Table 2**

Extracted parameters for characterizing the Bingham-Papanastasiou non-Newtonian fluidic meibum.

temperature T (°C)	minimum yield stress $\tau_y$ (N/m <sup>2</sup> )	plastic viscosity $\eta_p$ (Pa·s)	scale factor $m_p$ (s)
25	95.53	74.95	19.81
30	24.40	9.90	4.55
35	5.36	2.94	62.70 <sup>a</sup>
40	2.06	1.01	190.00 <sup>a</sup>

<sup>a</sup>The values of the  $m_p$  parameter obtained at 35 °C and 40 °C fell within the 95% confidence bounds of (-1962, 2086) and (-Inf, Inf), respectively.